



SPE 155476

The Importance of Slow Slip on Faults During Hydraulic Fracturing Stimulation of Shale Gas Reservoirs

Mark D. Zoback, SPE, Arjun Kohli, Indrajit Das and Mark McClure, SPE
Stanford University

Copyright 2012, Society of Petroleum Engineer

This paper was prepared for presentation at the Americas Unconventional Resources Conference held in Pittsburgh, Pennsylvania, USA, 5–7 June 2012.

This paper was selected for presentation by an SPE program committee following review of information contained in an abstract submitted by the author(s). Contents of the paper have not been reviewed by the Society of Petroleum Engineers and are subject to correction by the author(s). The material does not necessarily reflect any position of the Society of Petroleum Engineers, its officers, or members. Electronic reproduction, distribution, or storage of any part of this paper without the written consent of the Society of Petroleum Engineers is prohibited. Permission to reproduce in print is restricted to an abstract of not more than 300 words; illustrations may not be copied. The abstract must contain conspicuous acknowledgment of SPE copyright.

Abstract

We utilize several lines of evidence to argue that slow slip on pre-existing fractures and faults is an important deformation mechanism contributing to the effectiveness of *slick-water* hydraulic fracturing for stimulating production in extremely low permeability shale gas reservoirs. First, we carried out rate and state friction experiments in the laboratory using shale samples from three different formations with a large range of clay content. These experiments indicated that slip on faults in shales comprised of less than about 30% clay is expected to propagate unstably, thus generating conventional microseismic events. In contrast, in formations containing more than about 30% clay are expected to slip slowly. Second, we illustrate through modeling that slip induced by high fluid pressure on faults that are poorly oriented for slip in the current stress field is expected to be slow, principally because slip cannot occur faster than fluid pressure propagates along the fault plane. Because slow fault slip does not generate high frequency seismic waves, conventional microseismic monitoring does not routinely detect what appears to be a critical process during stimulation. Thus, microseismic events are expected to give only a generalized picture of where pressurization is occurring in a shale gas reservoir during stimulation which helps explain why microseismicity does not appear to correlate with relative productivity. We review observations of long-period-long-duration seismic events that appear to be generated by slow slip on mis-oriented fault planes during stimulation of the Barnett shale. Prediction of how pre-existing faults and fractures shear in response to hydraulic stimulation can help optimize field operations and improve recovery.

Introduction

Multi-stage hydraulic fracturing with *slick-water* in horizontal wells is an effective completion strategy for producing commercial quantities of natural gas from organic-rich shale gas formations. That said, the physical mechanisms responsible for reservoir stimulation are poorly understood. The prevalent paradigm is that diffusion of water out of the hydraulic fracture stimulates shear failure on multiple small, pre-existing fractures and faults in the shale. This shear slip creates a network of relatively permeable flow paths and thus enhances productivity from the extremely low permeability shale formations. Microseismic events recorded during hydraulic fracturing are evidence of this shear slip and the ‘clouds’ of microseismic events associated with multiple hydraulic fracturing stages in a well are generally assumed to define the stimulated rock volume (SRV) from which the gas is being produced (Warpinski et al., 2012). While this paradigm is generally useful, a simple mass balance calculation illustrates that the cumulative deformation associated with the microseismic events can account for only a small fraction of the production. In a single well, it has been shown that the number of microseismic events does not correlate with production from successive hydraulic fracturing stages (Moos et al., 2011). Production from five wells in the Barnett shale studied by Vermylen and Zoback (2011) does not correlate the number of microseismic events generated by hydraulic fracturing in each well even though the wells were stimulated in a similar manner.

In this paper we argue that slow slip on numerous fault planes is occurring in shale gas reservoirs during stimulation. In fact, we believe this is likely to be the dominant deformation mechanism during hydraulic stimulation. The shear deformation associated with the slowly slipping faults is expected to create a network of multiple permeable planes surrounding the induced hydraulic fractures. In the sections below, we first review evidence of

long-period long-duration seismic events that were detected during hydraulic fracturing stimulation of the Barnett shale that are indicative of slow slip on pre-existing faults. We then briefly review rate and state friction theory and present laboratory friction measurements on samples of the Barnett, Eagle Ford, Haynesville and Fort St. John shales that support the notion that the majority of slip on pre-existing fractures and faults in shale gas formations is expected to be characterized by stable sliding. We next demonstrate through dynamic rupture modeling how elevated fluid pressure during hydraulic fracturing induces slow shear slip on fractures and faults that are mis-oriented to the current stress field.

Evidence of Slow Slip

Das and Zoback (2011) report a series of long period and long duration (LPLD) seismic events observed during hydraulic fracturing operations in the Barnett shale described in Vermilyen and Zoback (2011). Figure 1 illustrates sudden bursts of energy with a duration 10-100 seconds in some of the spectrograms recorded during the microseismic recordings. This energy is most conspicuous between 10-80 Hz as shown clearly in Figure 1b, in which three of these events are plotted with an expanded time scale. In this frequency band, generally not considered in micro-seismic analysis, the recorded waveforms (Figure 1c) are similar to tectonic tremor observed in subduction zones and strike slip margins (Figure 1d). Tectonic tremor is typically observed between 1-15 Hz, a frequency band that is not well-recorded by the 15 Hz geophones used for the microseismic monitoring. GPS crustal deformation measurements during periods of tectonic tremor (and the migration of tremor) indicate that they result from slow slip on the subduction zone and strike slip faults at depth (Shelly et. al., 2006; Ide et. al, 2007).

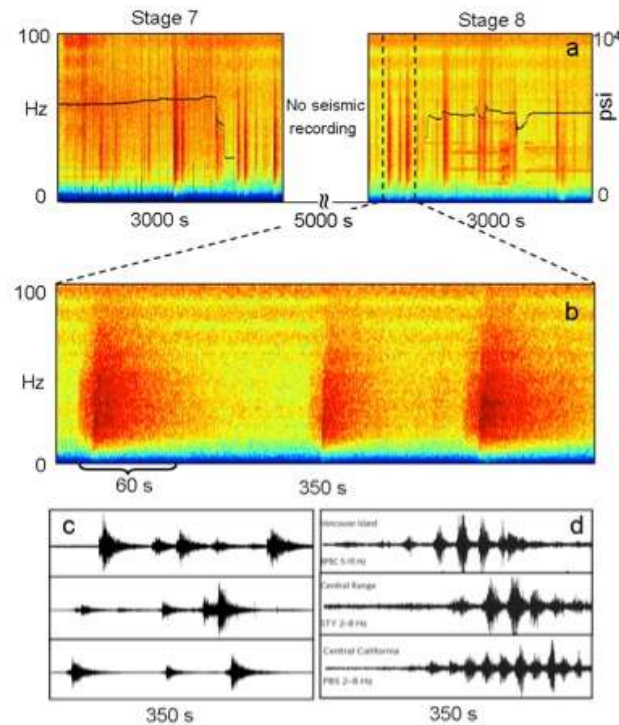


Figure 1: (a) Axial spectrogram of stage 8 during simultaneous fracturing of two wells in the Barnett shale. The small spikes at the bottom indicated times of reported microearthquakes. The black line shows the bottom-hole pressure during pumping. (b) LPLD events observed below 100 Hz. (c) Examples of filtered waveforms of LPLD events in this data set (10-80 Hz) (d) Examples of filtered tectonic tremor waveforms from Vancouver Island in British Columbia (5-15Hz), Central Range in Taiwan (2-8 Hz) and the SAF in Central California (2-8 Hz) (from Das and Zoback, 2011).

Das and Zoback (2011) proposed a hypothetical geometrical model (Figure 2) to explain the observations of LPLD events. From seismograms recorded on a borehole array in well C, they determined the directions from which the LPLD events originated. They propose that the events come from several pre-existing faults, parallel to those seen in the FMI log in well C, that cross-cut the hydrofrac planes created during the frac stages in wells A and B. The exact locations of the hydrofrac planes in any given stage is unknown, but they are expected to be perpendicular to S_{hmin} (and the well paths). They also show that the high pore pressure during pumping near the hydrofrac planes at the exact stages which recorded the largest number of LPLD events is able to activate slip on cross-cutting fault planes that are mis-oriented for slip in the current stress field. In other words, slip would not occur on these faults had pore pressure not been elevated during hydraulic fracturing.

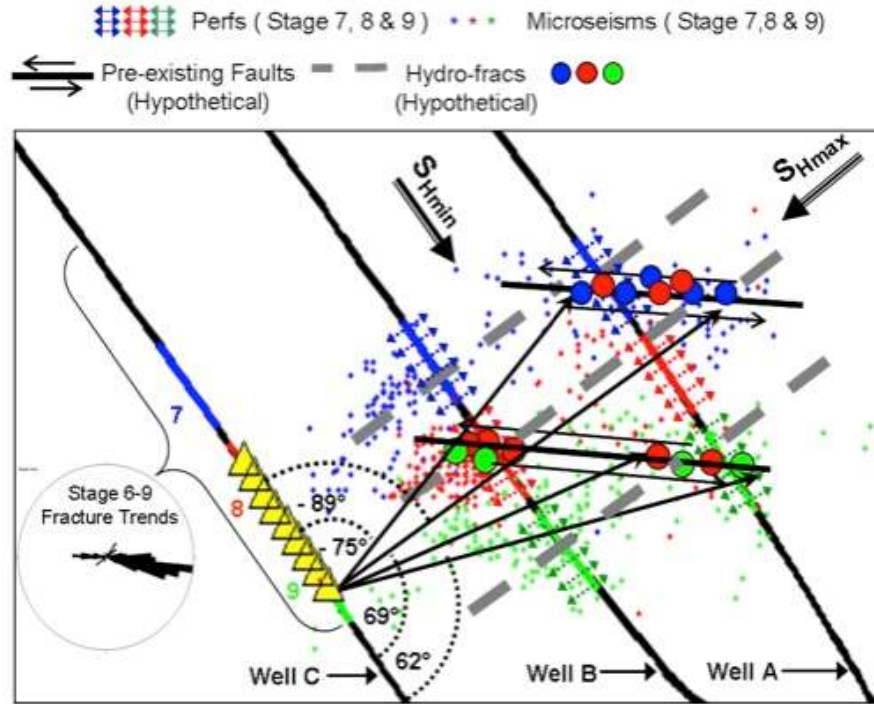


Figure 2: Interpretation of the origin of LPLD events recorded during hydraulic fracturing operations in the Barnett shale. From knowledge of the propagation direction of the LPLD events, they are interpreted to be associated with shear faults cross-cutting hydraulic fracturing planes (from Das and Zoback, 2011).

Laboratory Friction Experiments

Understanding the conditions responsible for induced seismic and slow slip events during stimulation stages requires the development of frictional stability criteria for shale gas reservoir rocks. Previous fault mechanics studies examining frictional stability have focused on clay-rich gouges, which are hypothesized to control the transition from seismic to slow or stable slip in the Earth through changes in mechanical and hydrologic properties with depth (Bird, 1984; Saffer and Marone, 2003). Initial laboratory studies have characterized the basic frictional strength of clay-rich gouges and demonstrate significant weakness in samples with clay contents as low as 15% (Shimamoto and Logan, 1981). Although previous studies of the frictional stability of clay-rich rocks have been carried out under specific conditions, no systematic investigations under the conditions (and rock types) relevant to reservoir stimulation of organic-rich shale gas formations have been previously presented.

To understand the observed slip behaviors during hydraulic fracturing operations in shales, a frictional constitutive law over the conditions of the reservoir is necessary. The Dietrich-Ruina rate and state constitutive laws (Ruina, 1983) have shown strong agreement with the results of laboratory rock friction studies on simulated fault gouge. The single-state variable form of the Dietrich-Ruina constitutive model is as follows:

$$\mu(V, \theta) = \mu_0 + a \ln(V/V_0) + b \ln(V_0 \theta) \quad (1)$$

$$d\theta/dt = (1 - V\theta/D_c) \quad (2)$$

$$(a - b) = \Delta\mu_{ss}/\ln(V/V_0) \quad (3)$$

in which μ_0 is the initial coefficient of friction, $\Delta\mu_{ss}$ is the change in the steady state coefficient of friction, a and b are material parameters representing the frictional evolution over a velocity step, V is the sliding velocity, V_0 is the initial sliding velocity, and θ is the state variable, which is sometimes represented as the average sliding contact lifetime at steady state. As illustrated in Figure 3, these changes are modeled to occur over a slip evolution displacement D_c , which represents the slip distance required to reach a new frictional steady state. In this formulation, the friction parameter $(a-b)$ is diagnostic of frictional evolution over a step-wise change in sliding velocity, with $(a-b) > 0$ describing a velocity-strengthening or stable response and $(a-b) < 0$ describing a velocity-weakening or potentially unstable response. In addition to the effect of frictional evolution, the slip behavior will be dependent on the effects of fluid pressure changes in the slipping zone.

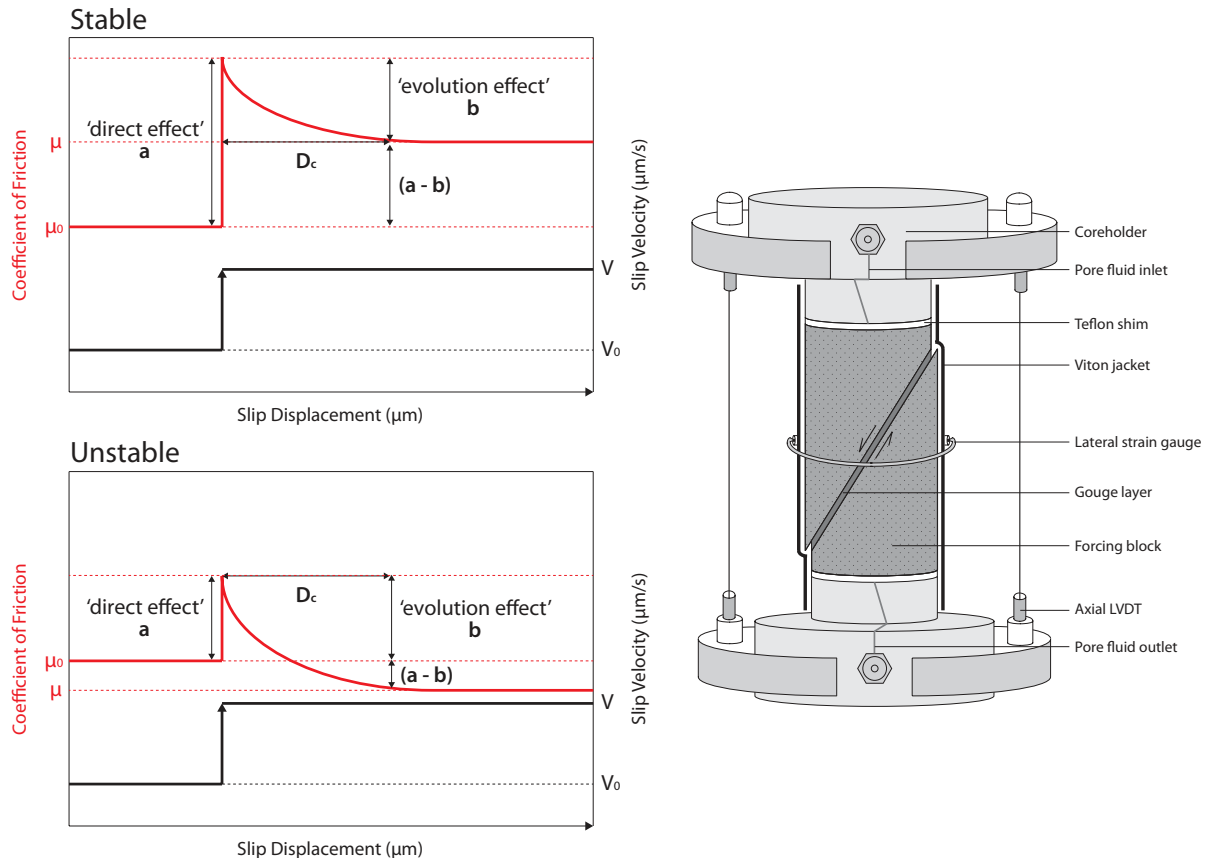


Figure 3: Schematic illustrations illustrating the principles of rate and state friction. In the upper diagram, an increase in sliding velocity of a fault is associated with an instantaneous increase in friction that evolves to a higher value of friction than acted initially. Such ‘velocity strengthening’ behavior, or $(a-b) > 0$, leads to stable sliding. The lower diagram illustrates ‘velocity weakening’ in which increasing slip velocity causes friction to evolve, to a lower value of friction than acted initially, leading to potentially unstable sliding.

Laboratory friction experiments were performed on gouge samples prepared from cores from the Barnett, Haynesville and Eagle Ford shale reservoirs as part of a methodology to measure frictional strength and rate and state constitutive parameters (Kohli and Zoback, 2011). Sliding velocities ranging from 0.1 – 10 $\mu\text{m/s}$ were implemented in approximately even displacement increments up to 5 mm, which represents the maximum allowed sliding displacement in this experimental geometry due to the presence of a Viton sample jacket around the sample. The sample setup is shown schematically on the right of Figure 3.

As shown in Figure 4, the coefficient of friction decreases monotonically from about 0.75 to 0.35 as the weight percent of clay plus kerogen increases to $\sim 60\%$. In addition, for samples with less than $\sim 30\%$ clay plus kerogen, $(a-b) < 0$ indicating unstable (seismic) sliding, whereas when there is more than $\sim 30\%$ clay plus kerogen, $(a-b) > 0$, indicating stable sliding. This threshold appears to be consistent for all three shale formations.

Microseismicity and Shale Composition

Figure 5 shows five wells in the Barnett shale shows and the resultant distribution of microseismic events recorded during hydraulic fracturing operations. Wells A, B and C are the same wells shown in Figure 2. The perforations, frac stages, pumping rates and volumes were the same for each stage although wells A and B (the two wells on upper right), were hydraulically fractured simultaneously by using twice as much pumping capacity (Vermylen and Zoback, 2011). It is noteworthy that the density of microseismic events is quite variable despite the uniformity of the stimulation process. The background color in Figure 5 represents a statistical interpolation of the gamma logs recorded in each well using sequential Gaussian simulation. While not a precise measure, gamma logs are a generally good indicator of clay content. Unfortunately, it is the only geophysical data available from all five wells. Note that where gamma is high (i.e., where clay content appears to be high), there are relatively few microearthquakes. This is especially clear near the toes of the wells and in the vicinity of stage 4 in wells A and B.

There are a number of ways in which clay content affects the physical properties of shale gas formations. For example, Sone and Zoback (2010) show that there is an increase in shale ductility with increasing clay content. For this reason, there may be fewer earthquakes in the high clay areas. However, one very appealing explanation for the lack of microseismic events in clay rich areas is the rate and state constitutive parameters shown in Figure 4. Where

clay content is low (samples corresponding to Barnett Light in Figure 4), slip is expected to be unstable ($a-b < 0$) on the small faults surrounding the hydraulic fractures producing numerous microearthquakes. Where clay content is high (Barnett Dark in Figure 4) slip on faults is expected to be stable ($a-b > 0$), resulting in relatively few microearthquakes in these regions. As explained in the next section, even when ($a-b < 0$) and fault slip is expected to be unstable, other factors affect whether slip is stable or not (Ikari et al., 2011). One critical factor is the orientation of a given fault with respect the prevailing stress field.

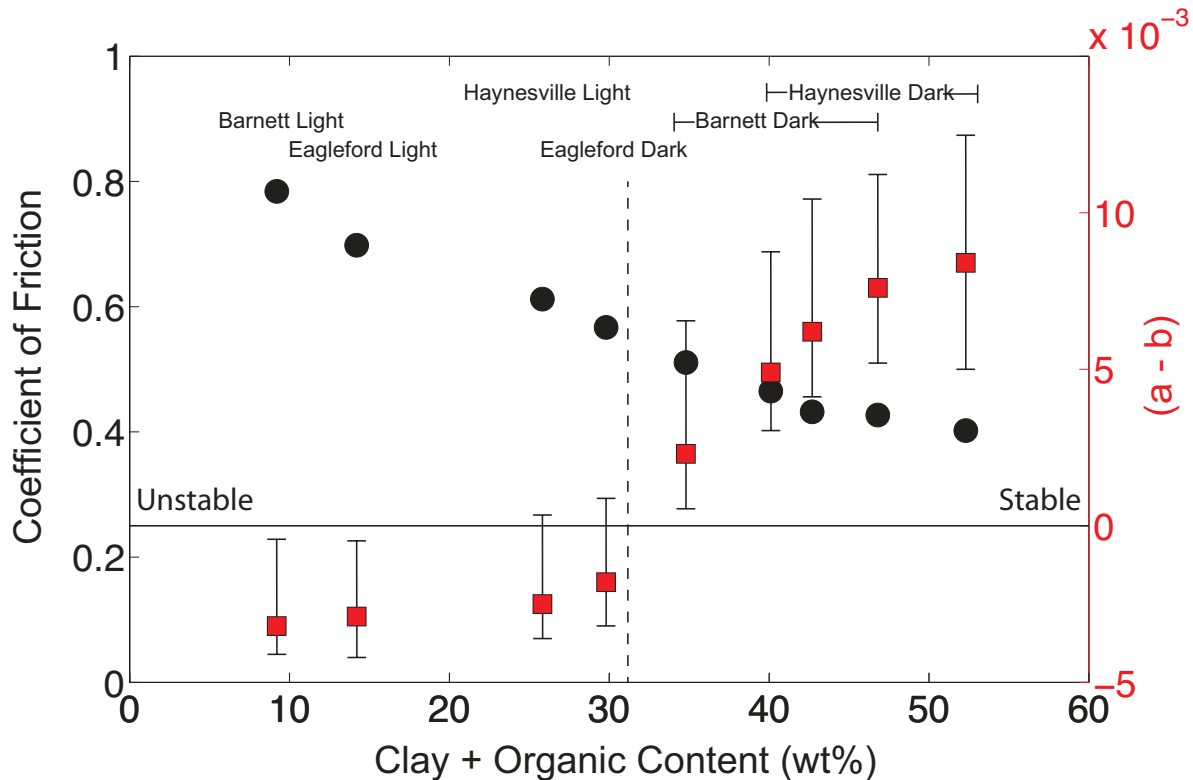


Figure 4: Variation of fault friction (black circles) and the stability parameter ($a-b$) (red squares) as a function of clay plus organic content in shale gas reservoir samples. Black bars show errors for values of ($a-b$). The specific reservoir for each sample is denoted by the labels above the datapoints. Note the transition from stable to unstable sliding at around 30% clay plus organic content.

Slow Slip on Mis-Oriented Faults

In fractured rock masses there are pre-existing fractures and faults at a variety of orientations. Some of these faults are likely to be well-oriented for slip in the ambient stress field, which are sometimes termed *critically-stressed* faults (Zoback, 2007). While faults that are *mis-oriented* for slip in the ambient stress field would normally not be expected to be capable of slipping, however, the strong elevation of fluid pressure during hydraulic fracturing is capable of triggering slip on mis-oriented faults. In this section, we demonstrate that induced slip on mis-oriented faults is expected to be slow slip, undetected in micro-seismic surveys. We argue below that slow slip on faults is likely to be a fundamental component of hydraulic stimulation.

The left side of Figure 6 shows an estimate of the minimum pore pressure perturbation induced in the reservoir during hydraulic fracturing of the five wells shown in Figure 5. Vermilyen and Zoback (2011) showed that the rapid pressurization that accompanied the simultaneous fracturing of wells A and B caused a large, poroelastic change in the least principal stress that increased with stage number and was most notable close to the heel areas of the wells. The largest poroelastic stress changes were observed in wells A and B because the frac stages were carried out in much less time than in the other wells. For example, wells A and B were fractured in 100 hours, whereas it took twice as long hydraulically fracture wells D and E, even though there were the same number of stages, rates and amounts of fluid, etc. Vermilyen and Zoback (2011) interpreted the increase of the least principal stress as a poroelastic effect because the effect was largest when the fluid pressure had the least amount of time to dissipate between hydraulic fracturing stages. As the pore pressure change that caused the stress change must be at least as large as the observed stress change, the values shown in the figure represent a lower bound estimate of the pore pressure change experienced by the reservoir during the multiple hydraulic fracturing stages in each well. The right side of Figure 6

shows the individual hydraulic fracturing stages and the locations and strike of faults and fractures observed in an FMI log in well C.

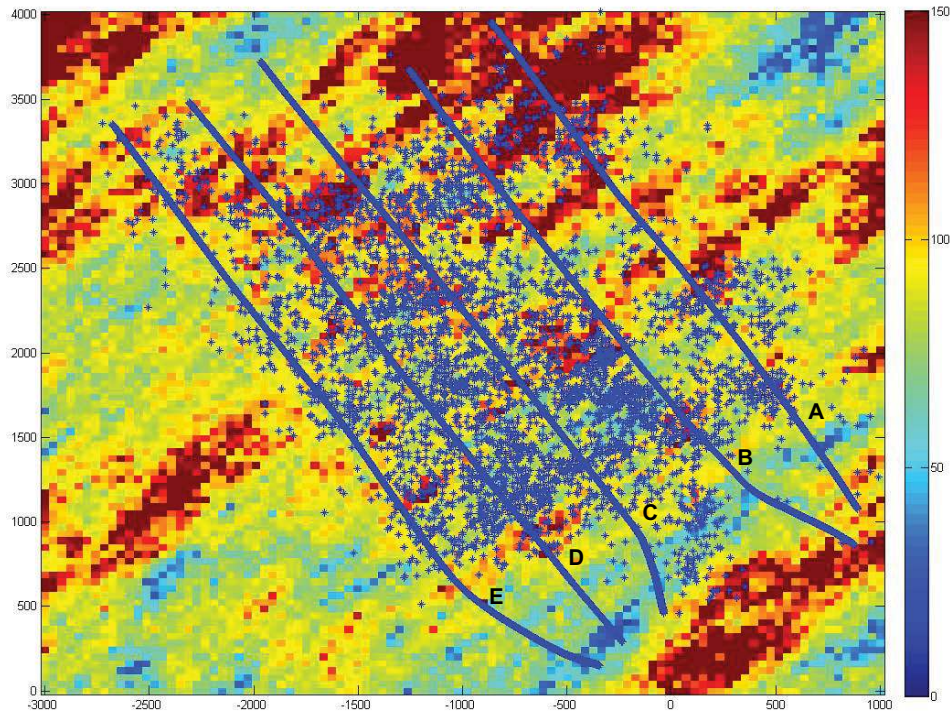


Figure 5: Five wells horizontal wells in the Barnett shale A, B, C, D and E with recorded micro-earthquakes shown by + symbols (as described by Vermynen and Zoback, 2011) superimposed on a statistical representation of gamma logs in the five wells using sequential Gaussian simulation. Gamma logs roughly correlate with clay content in these wells.

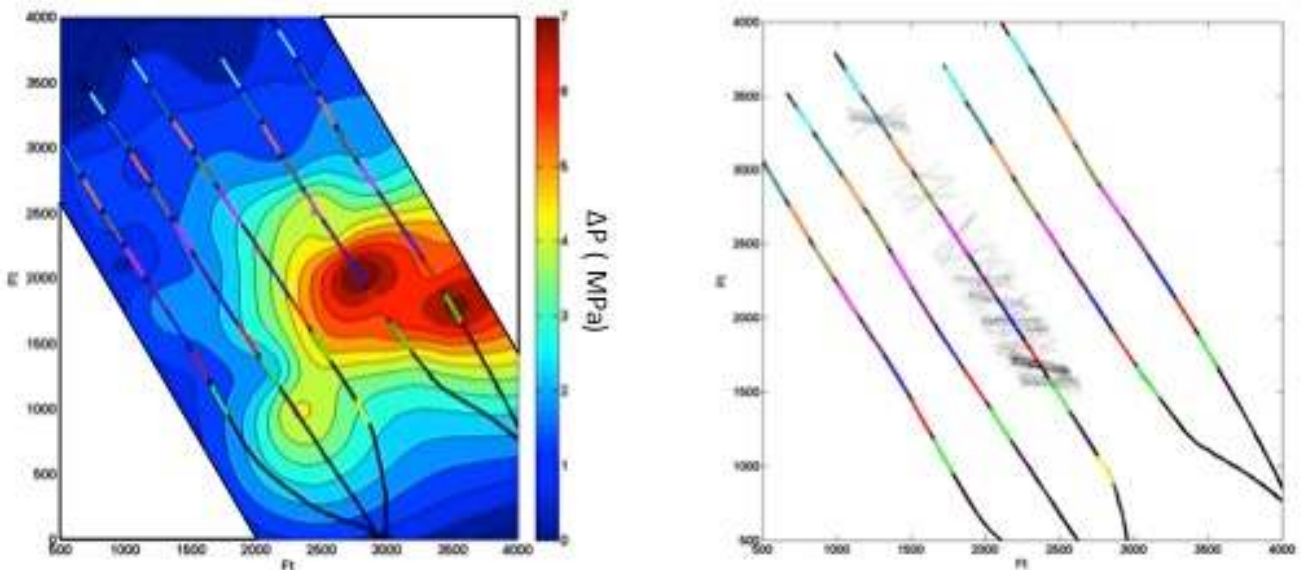


Figure 6: (Left) An estimate of the minimum pore pressure perturbation that affected the reservoir during hydraulic fracturing of the five wells in the Barnett shale previously shown in Figure 5. (Right) The individual hydraulic fracturing stages in the five wells and the strike direction of the natural fractures observed in well C with an FMI log.

Figure 7 shows how elevated pore pressure induces slip on poorly oriented faults utilizing the stress state determined for this reservoir. The vertical stress is the largest principal stress and the magnitudes of the two

horizontal principal stresses differ by only a few MPa. The direction of maximum horizontal compression is about N45°E. The stereonet in the upper left of the figure shows poles to pre-existing fracture and fault planes observed in well C. As shown, a wide variety of fracture and fault orientations are observed. The colored background of the stereonet shows the pressure needed to induce slip on the faults. As the initial pore pressure in the reservoir was about 18 MPa, only a few of the faults were close to being critically-stressed in the current stress field prior to stimulation. This is shown in the Mohr diagram in the lower left. The great majority of the fracture and fault planes are not close to shear failure and require several MPa of increased pore pressure to induce slip.

The map on the left side of Figure 6 shows that pore pressure changes during hydraulic fracturing were about 1-3 MPa through most of the reservoir affected by stimulation. As shown by the colors in the stereonet, slip would be induced on a small number of pre-existing faults by such pressure changes. As the maximum pressure changes in the reservoir during stimulation was about 6 MPa, the figures on the right side of Figure 7 shows what happens if pressure is increased by such a large amount. Note that the great majority of planes would be activated in shear.

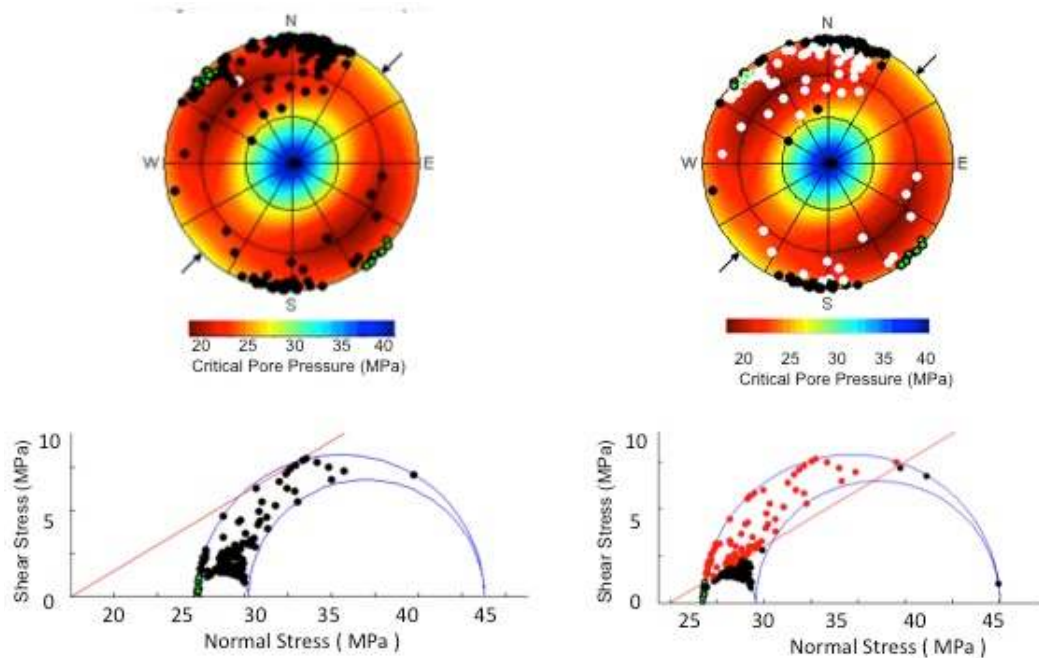


Figure 7: The left side of this diagram show the orientations of fractures and faults observed in well C under initial reservoir conditions. The stereonets show the orientation of fracture and fault planes and the color represents the pore pressure necessary to induce slip on the planes. The direction of maximum horizontal compression is also shown on the stereonets. The Mohr diagram in the lower left shows that only a few of the fracture and fault planes are active in the reservoir without stimulation. The stereonet and Mohr diagram on the right side shows that when pore pressure is perturbed by 6 MPa, slip would be induced on the great majority of the planes.

The fact that elevated pore pressure initiates slip on mis-oriented planes is well known from the basic principles of fault mechanics. What is not well known is that while slip on a critically-stressed fault could propagate rapidly as a microearthquake when triggered (assuming $(a-b) < 0$), induced slip on mis-oriented planes will propagate slowly and go undetected during normal microseismic surveys. Simply put, the reason for this is that slip on a portion of a mis-oriented fault will only occur where the pore pressure is anomalously high. Thus, slip will propagate along a mis-oriented fault only as rapidly as pore pressure propagates along it. Figure 8 shows a series of theoretical calculations to make this point.

The modeling utilizes the procedure described by McClure and Horne (2011) and incorporates fluid flow along the fault planes, rate and state friction and an associated change in permeability on the fault plane once slip is induced. The faults of various orientations were considered in the model. As in the case shown in Figure 7, a few of the pre-existing fracture and fault planes are critically-stressed under normal reservoir conditions but the great majority of the fracture and fault planes will not slip unless fluid pressure is increased.

Figure 8 shows the evolution of pore pressure and slip on a mis-oriented fault. The faults are 5 m in length and it is assumed the slip is initiated at the center of the fault. The left panel is slip velocity, the center panel is pore pressure and the right panel shows faults displacement. While the exact values in these figures are highly dependent on poorly constrained parameters used in the model such as permeability and the change in permeability with displacement, the calculations are instructive in illustrating how slip evolves on a mis-oriented fault. Note that high pressure acting in

the middle of the fault (center panel) initiates a small amount of slip at the middle of the fault (right panel). As time goes on and pressure spreads out along the fault, the velocity of slip (left panel) increases as well as the amount of displacement. As pore pressure reaches the ends of the fault, displacement reaches its maximum value and the slip velocity slows down.

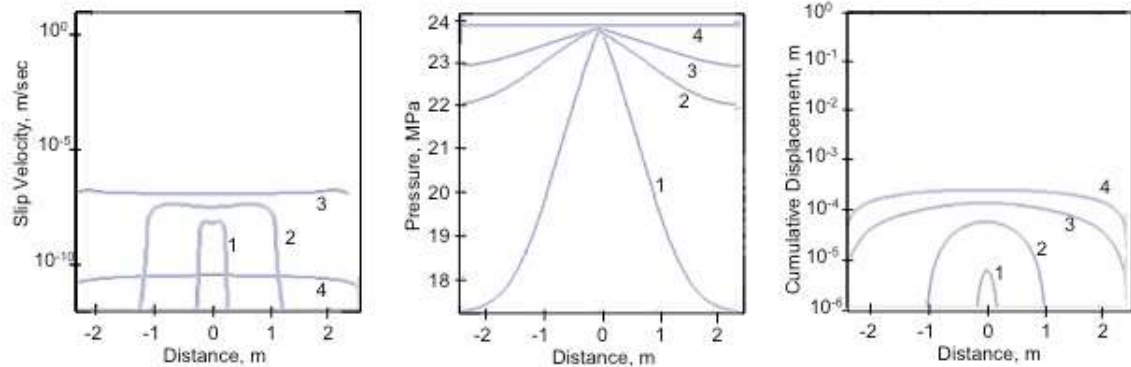


Figure 8: Evolution of slip on a mis-oriented fault. The left panel shows slip velocity, the center panel shows pore pressure and the right panel shows displacement. 1, 2, 3 and 4 indicate successive times as pore pressure spreads out along the fault and displacement increases. While the exact values in these figures are highly dependent on parameters used in the model, they illustrate how slip evolution is dependent on the rate at which pore pressure increases along the fault.

Figure 9 summarizes the results of modeling illustrated in Figure 8 on faults of a wide variety of orientations. Except for fault orientation, the parameters used in all of the calculations are the same. The color of the symbol indicates the speed of rupture propagation. The red symbols indicate the triggering of seismic slip on faults that are well-oriented for slip (critically-stressed under initial reservoir conditions). In all cases $(a-b) < 0$ indicating that slip could potentially be unstable. What is observed, however, is that the triggered slip is slow on the faults that are mis-oriented faults to the current stress field (as shown in purple). For the friction parameters and pore pressure perturbation used in the calculations, slip does not occur on the most severely mis-oriented faults.

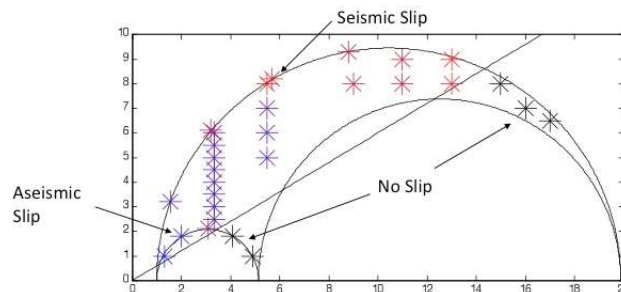


Figure 9: Summary of calculations on faults of various orientations indicating whether faults slip seismically or aseismically when triggered by fluid pressure. Each calculation is similar to the modeling illustrated in Figure 8. Well-oriented (critically-stressed) faults are expected to slip seismically (as $(a-b) < 0$ in these calculations) whereas mis-oriented faults slip slowly. Severely mis-oriented faults do not slip for the parameters used in the modeling.

Conclusions

It is well known that there is great variability in the productivity of shale gas wells in a given area. Not only are many wells not economic, it is frequently argued that the great majority of gas produced in a given well comes from only a few of the fracturing stages. We argue here that pervasive slow slip on faults may be critical during hydraulic fracturing if it is to be effective in stimulating production from extremely low permeability shale gas reservoirs. If this is the case, it is important to approach shale gas development from a predictive perspective rather than carrying out the hydraulic fracturing with a pre-determined regularized spacing, volumes and rates. Mapping the distribution of fractures and faults in a reservoir, developing an understanding of the magnitude and orientation of the three principal stresses and predicting the pressure at which slip will be induced on mis-oriented faults can be accomplished with well-established technologies (Zoback, 2007). Utilizing such knowledge, it is possible to design reservoir stimulation in a manner that is both optimally efficient and most productive.

Acknowledgements

We thank ConocoPhillips for making the Barnett shale data available that was used in this study, Baker RDS for

allowing us to use GMI software for the calculations shown in Figure 7 and Elnur Aliyev and Kurt Wilson for generating the image in Figure 5. The samples used in this study came from ConocoPhillips and BP. The Stanford Rock and Borehole Consortium, ConocoPhillips and Chevron provided financial support for this work. Arjun Kohli received financial support via a Graduate Fellowship from the U.S. National Science Foundation.

References

- Bird, P., 1984. Hydration-phase diagrams and friction of montmorillonite under laboratory and geologic conditions, with implications for shale compaction, slope stability, and strength of fault gouge, *Tectonophysics*, 107, pp. 235- 260.
- Das, I. and M.D. Zoback, 2011. Long-period, Long-duration Seismic Events During Hydraulic Fracturing Stimulation of a Shale Gas Reservoir, *The Leading Edge*, July, 2011.
- Ikari, M.J., Marone, C., and D.M. Saffer, 2011. On the relation between fault strength and frictional stability. *Geology*, v. 39, pp. 83- 86.
- Kohli, A.H., and M.D. Zoback, 2011. Rate-state frictional properties of shale reservoir rocks. American Geophysical Union Fall Meeting, T23C-1944.
- McClure, M. W. and R. N. Horne, 2011. Investigation of injection-induced seismicity using a coupled fluid flow and rate/state friction model, *Geophysics*, 76 (6), WC181-WC198.
- Moos, D., G. Vassilellis, R. Cade, J. Franquet, A. Lacazette, E. Bourtembourg and R. Cade, 2011. Predicting shale reservoir response to stimulation in the upper Devonian of West Virginia. Paper SPE-145849, SPE Annual Technical Conference and Exhibition held in Denver, Colorado, USA 30 October-2 November, 2011.
- Ruina, A., 1983. Slip Instability and State Variable Friction Laws. *J. Geophys. Res.* Vol. 88, pgs. 10,359-10,370.
- Saffer, D.M. and C. Marone, 2003. Comparison of smectite- and illite- rich gouge frictional properties: Application to the updip limit of the seismogenic zone along subduction megathrusts, *Earth and Planetary Science Letters*, 215, 219-235.
- Shimamoto, T., and J.M. Logan, 1981. Effects of simulated clay gouges on the sliding behavior of Tennessee Sandstone. *Tectonophysics*, 75, pp. 243 – 255.
- Sone, H. and M.D. Zoback, 2010, Strength, creep and frictional properties of gas shale reservoir rocks. Paper ARMA- 10-463, 44th US Rock Mechanics Symposium and 5th U.S.-Canada Rock Mechanics Symposium, held in Salt Lake City, UT June 27–30, 2010.
- Vermilyen, J. P. and M.D. Zoback, 2011. Hydraulic fracturing, microseismic magnitudes, and stress evolution in the Barnett shale, Texas, USA, SPE- 140507, paper was prepared for presentation at the SPE Hydraulic Fracturing Technology Conference and Exhibition held in The Woodlands, Texas, USA, 24–26 January 2011.
- Warpinski, N.R., J. Du and U. Zimmer, 2012. Measurements of hydraulic-fracture-induced seismicity in gas shales. Paper SPE-151597, SPE Hydraulic Fracturing Technology Conference held in The Woodlands, Texas, USA 6-8 February 2012.
- Zoback, M.D., 2007. *Reservoir Geomechanics*, Cambridge University Press, 459 pp.